Monthly Notices
of the
ROYAL ASTRONOMICAL SOCIETY

MNRAS **480,** 1340–1352 (2018)
Advance Access publication 2018 July 20

doi:10.1093/mnras/sty1941

The environment of radio galaxies: a signature of AGN feedback at high redshifts

David Izquierdo-Villalba,[1]★ Álvaro A. Orsi,[1] Silvia Bonoli,[1] Cedric G. Lacey,[2] Carlton M. Baugh[2] and Andrew J. Griffin[2]

[1] *Centro de Estudios de Física del Cosmos de Aragón (CEFCA), Plaza San Juan 1, Planta-2, Teruel E-44001, Spain*
[2] *Institute for Computational Cosmology, Department of Physics, University of Durham, South Road, Durham DH1 3LE, UK*

Accepted 2018 July 19. Received 2018 July 19; in original form 2017 December 19

ABSTRACT

We use the semi-analytical model of galaxy formation GALFORM to characterize an indirect signature of active galactic nucleus (AGN) feedback in the environment of radio galaxies at high redshifts. The predicted environment of radio galaxies is denser than that of radio-quiet galaxies with the same stellar mass. This is consistent with observational results from the CARLA survey. Our model shows that the differences in environment are due to radio galaxies being hosted by dark matter haloes that are ∼1.5 dex more massive than those hosting radio-quiet galaxies with the same stellar mass. By running a control simulation in which AGN feedback is switched off, we identify AGN feedback as the primary mechanism affecting the build up of the stellar component of radio galaxies, thus explaining the different environment in radio galaxies and their radio-quiet counterparts. The difference in host halo mass between radio-loud and radio-quiet galaxies translates into different galaxies populating each environment. We predict a higher fraction of passive galaxies around radio-loud galaxies compared to their radio-quiet counterparts. Furthermore, such a high fraction of passive galaxies shapes the predicted infrared luminosity function in the environment of radio galaxies in a way that is consistent with observational findings. Our results suggest that the impact of AGN feedback at high redshifts and environmental mechanisms affecting galaxies in high halo masses can be revealed by studying the environment of radio galaxies, thus providing new constraints on galaxy formation physics at high redshifts.

Key words: galaxies: active – methods: numerical – galaxies: high-redshift – radio continuum: galaxies.

1 INTRODUCTION

Within the current picture of galaxy formation, an active galactic nucleus (AGN) is associated with the energy release resulting from gas accretion onto supermassive black holes (SMBH) residing at the centre of most galaxies (Soltan 1982; Kormendy & Richstone 1995; Richstone et al. 1998; Kormendy & Gebhardt 2001). Nuclear activity is thought to impact star formation through different physical processes [such as the heating and compression of the intergalactic medium (IGM)], to refer to which the community uses the general term 'AGN feedback' (Silk & Rees 1998; Bîrzan et al. 2004; Di Matteo, Springel & Hernquist 2005; Springel 2005; Diamond-Stanic & Rieke 2012; Mullaney et al. 2012a,c; Chamani, Doerschner & Schleicher 2017; Eisenreich et al. 2017; Shabala et al. 2017).

In galaxy formation models, AGN feedback is invoked to heat the gas content of massive galaxies and their host dark matter haloes, thereby quenching star formation and regulating the abundance of bright, massive galaxies (see e.g. Benson et al. 2003; Granato et al. 2004; Bower et al. 2006; Croton et al. 2006; Cattaneo et al. 2007). In this context, theoretical models typically distinguish between two types of AGN feedback: the radiative 'quasar mode', associated with episodes of efficient cold gas accretion onto the central black hole (BH), which is typically triggered by galaxy mergers or disc instabilities, and the 'radio mode', which depends directly on gas accretion from the hot halo surrounding galaxies and is responsible for powering relativistic jets (Bower et al. 2006; Croton et al. 2006; Cattaneo et al. 2007; Lagos, Cora & Padilla 2008; Somerville et al. 2008; Fanidakis et al. 2012, 2013a; Henriques et al. 2015). Recent hydrodynamical simulations have shown that AGN feedback can shape the central mass distribution of the host galaxies and induce the quenching of star formation (Di Matteo et al. 2005; Booth &

★ E-mail: dizquierdo@cefca.es

Schaye 2009; Bonoli et al. 2016; Dubois et al. 2016; Spinoso et al. 2017; Weinberger et al. 2017).

Despite its key role in models, AGN feedback and its impact on galaxy evolution is not well characterized observationally. Studies have not reached conclusive results when they have tried to explore correlations between AGN luminosity (in the X-ray, optical, or radio bands) and host properties such as star formation rates (SFRs) and BH accretion (Hardcastle, Evans & Croston 2006; Best et al. 2007; Shao et al. 2010; Georgakakis et al. 2011; Harrison et al. 2012; Mullaney et al. 2012b; Rodighiero et al. 2015; Stanley et al. 2015; Lanzuisi et al. 2017; Soergel et al. 2017). Furthermore, feedback processes like outflows and winds are extremely difficult to observe (see e.g. Bischetti et al. 2017). Despite the difficulties, some studies have been able to detect signs that AGN outflows interact with the interstellar medium (ISM), warming up the gas (see Nesvadba et al. 2008; Guillard et al. 2012; Morganti et al. 2013). Numerical simulations of relativistic jets have been carried out showing that jets via bow shocks inject thermal energy in the ISM and expel a large amount of host galaxy gas (Perucho, Quilis & Martí 2011; Wagner & Bicknell 2011; Wagner, Bicknell & Umemura 2012; Wagner, Umemura & Bicknell 2013; Perucho et al. 2014). Even more, new relativistic magnetohydrodynamic simulations (GRMHD) have tried to give a more accurate phenomenological law for jet powers (Zamaninasab et al. 2014; Tchekhovskoy 2015) and unified the AGN feedback processes (Gaspari & Sądowski 2017; Gaspari et al. 2018).

Following the above, some recent studies have focused on high-z radio-loud AGNs (RLAGNs) to prove the existence of a co-evolution between AGNs and their host galaxies (Holt, Tadhunter & Morganti 2008; Nesvadba et al. 2008). RLAGNs are expected to be good candidates to trace AGN feedback since they (i) sample some of the most massive galaxies at high-z (Seymour et al. 2007); (ii) lie in overdense regions (Hill & Lilly 1991; Pascarelle et al. 1996; Best 2000; Kurk et al. 2000, 2004a,b; Venemans et al. 2004; Hatch et al. 2011, 2014; Cooke et al. 2014; Orsi et al. 2016); and (iii) are associated with energetic outflows of ionized gas powered by their central SMBHs (Nesvadba et al. 2008, 2017). Recently, the CARLA survey has targeted the environment of high-z RLAGNs (Wylezalek et al. 2013, 2014; Cooke et al. 2015, 2016). Their results show that radio galaxies (RGs), a sub-sample of RLAGNs, lie in denser environments with respect to radio-quiet galaxies with the same stellar mass (Hatch et al. 2014). This result suggests a link between the environment and the physical processes connected with the radio activity.

Here, we explore this link from a theoretical perspective. We use the GALFORM galaxy formation and evolution model (Cole et al. 2000; Bower et al. 2006; Lacey et al. 2016) to study the environment of radio-loud and radio-quiet galaxies and explore the physical mechanisms that lead to differences in the environment of the two populations. We compare the model predictions with the results obtained from the CARLA survey. As the model includes AGN feedback, we can explore how black hole growth affects the evolution of massive galaxies at high redshifts.

The outline of this work is as follows. In Section 2, we briefly describe the galaxy formation model used. In Section 3, we study the predicted environment of radio-active and radio-quiet galaxies and investigate how the differences are due to the role of AGN feedback. In Section 4, we focus on the properties of galaxies surrounding RGs. Finally, in Section 5 we summarize our main findings. Magnitudes are given in the absolute (AB) system and distances in comoving units.

2 GALAXY FORMATION MODEL

Throughout this work, we make use of the semi-analytical model of galaxy formation GALFORM. A full description of the model can be found in Cole et al. (2000), Benson et al. (2003), Baugh et al. (2005), Bower et al. (2006), and Lacey et al. (2016). We use here the latest variant of the model, described in Lacey et al. (2016), and the modifications presented in Baugh et al. (in preparation) and Griffin et al. (2018). In brief, GALFORM computes the formation and evolution of the galaxy population set in a hierarchical structure formation scenario. The main physical processes driving galaxy formation and BH evolution include gas cooling and disc formation in dark matter (DM) halos, leading to star formation in the disc component and to subsequent regulating mechanisms such as supernova and AGN feedback; chemical enrichment of the gas and stars; galaxy mergers and disc instabilities leading to bursts of star formation and the formation of a spheroid component; the evolution of SMBHs and the computation of observed properties such as AGN and galaxy luminosities. The GALFORM variant in Lacey et al. (2016) shows good agreement with a wide range of galaxy proprieties, such as their luminosity and stellar mass function, the evolution of Lyman break galaxies, galaxy sizes, and the number counts of submillimetre galaxies at $z > 2$.

In this work, we run GALFORM in the P-MILLENNIUM N-body simulation (Baugh et al. in preparation). This large simulation has a halo mass resolution of $2.12 \times 10^9\ \mathrm{M}_\odot\, h^{-1}$, corresponding to 20 simulation particles, each with mass $1.06 \times 10^8\ \mathrm{M}_\odot\, h^{-1}$, a periodic box of $542.16\,\mathrm{Mpc}\, h^{-1}$, and cosmological parameters consistent with the latest cosmological constraints from the *Planck* mission (Planck Collaboration 2016): $\Omega_\mathrm{M} = 0.307$, $\Omega_b = 0.0483$, $\Omega_\Lambda = 0.677$, $\mathrm{n_s} = 0.968$, $\sigma_8 = 0.8288$, and $h = 0.677$. The model parameters are retuned slightly compared with those used in Lacey et al. (2016), to compensate for the change in the cosmological parameters, the improved simulation resolution, and a new galaxy merger scheme (Campbell et al. 2015; Simha & Cole 2016; Baugh et al. in preparation).

The modelling of SMBH in GALFORM was introduced in Malbon et al. (2007) and then extended to include AGN feedback by Bower et al. (2006), Fanidakis et al. (2012, 2013a), and Griffin et al. (2018). The model includes three channels in which BHs can grow: *mergers* with other BHs, gas accretion during the *starburst mode* (or *quasar mode*), and the *hot-halo mode* (or *radio mode*). The *starburst* mode is triggered by disc instabilities or galaxy mergers; during these processes, a large amount of cold gas is expected to be driven towards the inner parts of the galaxy, providing fuel for the BH. The *hot-halo* mode assumes that the gas is accreted onto the BH directly from the diffuse quasi-static hot gas atmosphere of the DM halo, without being cooled onto the galactic disc.

To prevent the formation of an excess of massive galaxies, GALFORM introduces a star formation quenching process via AGN feedback. This mechanism is triggered during the BH hot-halo growth phase (radio feedback). During this phase, the BH injects thermal energy isotropically in the galaxy hot-halo atmosphere, delaying or even stopping its cooling flow. The radio mode quenches the star formation in a galaxy when (i) the cooling time of hot gas is larger than the free-fall time and (ii) the BH accretion is significantly sub-Eddington ($f_\mathrm{Edd} < 0.01$[1]), to balance the radiative luminosity of the cooling flow. Both conditions are satisfied in haloes with

[1]Where f_Edd is defined as the ratio between the bolometric (L_bol) and Eddington (L_Edd) luminosity of the accreting BH.

masses $\sim 10^{11.8}\,\mathrm{M}_{\odot}\,h^{-1}$ (see Bower et al. 2006; Fanidakis et al. 2011; Lacey et al. 2016; Mitchell et al. 2016).

The code computes the gas accreted by the BH via the *starburst* and *hot-halo* modes at every time-step, and converts it into an accretion rate $\dot{M}$. In the *starburst* mode, the duration of the accretion episode is proportional to the dynamical time-scale of the host spheroid while in the *hot-halo* mode it is computed using the time-step over which the gas is accreted from the halo atmosphere. The accretion disc bolometric luminosity ($L_{\rm bol}$) is calculated with the Shakura–Sunyaev thin-disc (TD) solution (Shakura & Sunyaev 1973) if the value of $\dot{M}$ in Eddington units ($\dot{m} = \dot{M}/\dot{M}_{\rm Edd}$) exceeds a critical accretion rate of $\dot{m}_{\rm c} = 0.01$. On the other hand, when $\dot{m} \leq \dot{m}_{\rm c}$, the advection-dominated accretion flow (ADAF) thick-disc solution is adopted (Narayan & Yi 1994). The thin-disc accretion channel is linked with the fast rate of BH growth while the ADAF is linked with the slow rate of growth and usually connected with the feedback phase implemented in the model. Finally, if the accretion rate becomes supper-Eddington, the bolometric luminosity is limited to a factor proportional to the Eddington luminosity (see Fanidakis et al. 2011; Griffin et al. 2018).

The accretion flow forms a disc around the BH that is able to produce a relativistic jet whose power depends strongly on the disc structure (TD or ADAF), the BH mass and its spin (Meier 2002; Fanidakis et al. 2011):

$$L_{\rm jet,ADAF} = 2\times10^{45}\left(\frac{M_{\rm BH}}{10^9\,\mathrm{M}_{\odot}}\right)\left(\frac{\dot{m}}{\dot{m}_{\rm c}}\right)a^2 \quad [\mathrm{erg\,s^{-1}}], \tag{1}$$

$$L_{\rm jet,TD} = 2.5\times10^{43}\left(\frac{M_{\rm BH}}{10^9\,\mathrm{M}_{\odot}}\right)^{1.1}\left(\frac{\dot{m}}{\dot{m}_{\rm c}}\right)^{1.2}a^2 \quad [\mathrm{erg\,s^{-1}}], \tag{2}$$

where $M_{\rm BH}$ and a are, respectively, the BH mass and spin. Given that the semi-analytical approx used here to compute the jet luminosity does not include any angular dependence, the model assumes an isotropic jet emission. In the super-Eddington regime, it is assumed that the flow remains in a thin-disc state as there is as yet no model to describe the behaviour of the radio jet in this regime.

The jet luminosities can be related to radio luminosities ($L_{\nu\rm R}$) using the non-linear dependence between the jet power and black hole mass ($M_{\rm BH}$) and accretion rate ($\dot{m}$) parameters (Heinz & Sunyaev 2003):

$$\nu_{\rm R}L_{\nu\rm R,ADAF} = A_{\rm ADAF}L_{\rm jet,ADAF}\left(\frac{M_{\rm BH}}{10^9\,\mathrm{M}_{\odot}}\frac{\dot{m}}{\dot{m}_{\rm c}}\right)^{0.42}, \tag{3}$$

$$\nu_{\rm R}L_{\nu\rm R,TD} = A_{\rm TD}L_{\rm jet,TD}\left(\frac{M_{\rm BH}}{10^9\,\mathrm{M}_{\odot}}\right)^{0.32}\left(\frac{\dot{m}}{\dot{m}_{\rm c}}\right)^{-1.2}, \tag{4}$$

where the normalization factors $A_{\rm TD}$ and $A_{\rm ADF}$ are adjustable parameters, set to 0.8 and 2×10^{-5}, respectively, in order to match the radio luminosity function at $z = 0$.

The dual solution presented in equations (1)–(2) and (3)–(4) gives a dichotomy in radio properties that is able to explain the distinction between radio-loud and radio-quiet objects. A powerful radio luminosity can be triggered by the two accretion regimens, ADAF and TD. For the former, we need a very massive and spinning BH whose accretion rate $\dot{m}$ needs to be very close to the maximum allowed for an ADAF to occur ($\sim \dot{m}_{\rm c}$). For the latter, the radio luminosity does not depend on the accretion rate and it is the BH mass and its spin that play the main role in triggering powerful radio luminosities. Finally, since the AGN feedback introduced by GALFORM only takes place in the BH *hot-halo* growth state during very sub-Eddington accretion rates ($\dot{m} < \dot{m}_{\rm c}$) the AGN feedback phase is only linked with the ADAF regimen.

3 THE ENVIRONMENT OF RADIO GALAXIES

In this section, we explore the GALFORM predictions for the typical overdensities around radio galaxies at z= 1.5, 2.2, and 3. We then discuss our results in the context of AGN feedback and compare our theoretical findings with the results of the CARLA survey.

3.1 The overdensities around radio galaxies

In a hierarchical structure formation scenario, overdensities around DM haloes are an increasing function of halo mass (e.g. Bardeen et al. 1986). At the same time, more massive galaxies are expected to live in more massive haloes, unless some baryonic process, such as feedback, is able to prevent stellar growth while dark matter haloes keep accreting mass (Benson et al. 2003). If AGN feedback prevents the stellar mass build up of radio galaxies, we expect them to be typically hosted by haloes more massive than what the average $M_{\rm stellar} - M_{\rm halo}$ relation would predict. Such a difference in the host halo masses of radio galaxies and radio-quiet galaxies with the same stellar mass should thus be reflected in the overdensities around the two populations.

To test this idea, we select a sample of central[2] RGs from the output of the model, calculate the overdensity of galaxies around these RGs, and compare the results against those predicted for two control samples of central galaxies matched either in stellar mass ($\mathrm{C_{M_S}}$) or in host halo mass ($\mathrm{C_{M_H}}$). To define the sample of RGs, we choose the 1 per cent brightest central galaxies in radio luminosity at ν = 1.4GHz predicted by GALFORM at each redshift. With this selection, we obtain 1156 objects at z= 1.5, 1806 objects at z= 2.2, and 2306 objects at z= 3.0. We explore the model predictions at these three different redshifts, as this is where the environments of radio galaxies have been characterized observationally (Wylezalek et al. 2013, 2014; Hatch et al. 2014; Cooke et al. 2015, 2016). Fig. 1 shows examples of the spatial distribution of dark matter subhaloes and galaxies around two radio galaxies and two galaxies from the $\mathrm{C_{M_S}}$ sample with comparable stellar masses at z= 2.2. RGs are embedded in a dense filamentary web of DM, where most of the neighbouring galaxies are typically not necessarily satellites of the central object but rather close neighbours that may belong to a different parent halo than the central object. The green contours in the figure highlight the projected surface density of subhaloes, showing that RGs are located in denser dark matter regions than that of the control sample galaxy.

The galaxy overdensity profile $\delta(r)$ around the radio galaxies and the galaxies of the two control samples is defined as

$$\delta(r) = \frac{n\,(<r)}{\bar{n}} - 1\,, \tag{5}$$

where $n\,(<r)$ $\mathrm{Mpc^{-3}}\,h^3$ is the number density of galaxies within a sphere of radius r around the target galaxy and $\bar{n}$ $\mathrm{Mpc^{-3}}\,h^3$ is the average number density of galaxies across the simulation box.[3]

[2]The term 'central' refers to galaxies that are located at the centre of their host dark matter halo (Springel 2005).

[3]To calculate the number of galaxies around target objects and the average number density of galaxies across the simulation box, we included all galaxies in the simulation with $M_{\rm stellar} \geq 10^9\ \mathrm{M}_{\odot}\,h^{-1}$. We have checked that a different choice for this lower limit in stellar mass does not affect our results (see Appendix A).

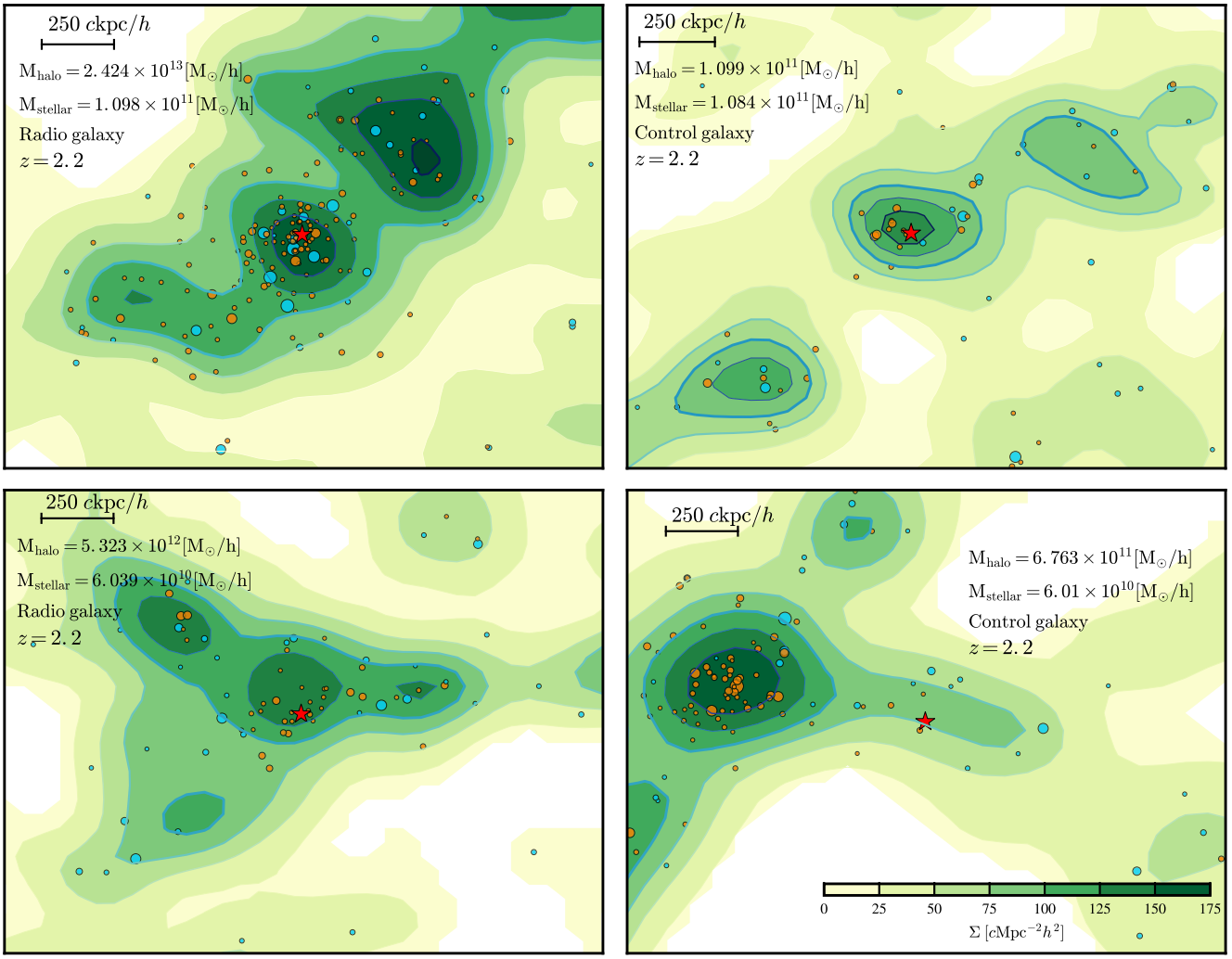

Figure 1. Examples of the environment of two RGs (left panels) and two galaxies from the control C_{M_S} sample (right panels) at z= 2.2. The red stars located at the centre of each panel indicate the position of the RG or the C_{M_S} galaxy, with stellar and host halo masses indicated on the panels. Circles indicate the positions of neighbouring galaxies, with the symbol size being proportional to the stellar mass of each galaxy, while the colour encodes the specific star formation rate (sSFR) of the galaxy: Orange circles indicate passive galaxies, while cyan symbols indicate star-forming galaxies, where the threshold between the two populations has been set to an sSFR value of 10^{-10} yr^{-1}. The contours represent the projected surface density of subhaloes around the central galaxy. The thickness of the projection is 5 $c$kpc h^{-1} and the length scale is indicated by the legend.

Fig. 2 shows the predicted galaxy overdensities around RGs compared to the C_{M_S} and C_{M_H} samples at the three different redshifts analysed. These results correspond to the ideal case in which no projection effects affect the measured overdensities. Our model predicts that RGs are typically surrounded by denser environments than galaxies with the same stellar mass distribution. The difference is slightly more pronounced at lower redshifts and at small scales ($r \lesssim 2$ Mpc h^{-1}), where the median of the distribution associated with radio galaxies is about an order of magnitude higher than that for the C_{M_S} control sample. At larger scales, the overdensity profiles start to converge [and $\delta(r)$ will eventually reach zero, by construction, at scales of several tens of cMpc h^{-1}]. There are no noticeable differences between the typical overdensities around radio galaxies and the galaxies of the C_{M_H} sample at any redshift.

To identify the mechanism causing the differences in the environment of RGs and the C_{M_S} sample, Fig. 3 (upper row) shows their halo mass distribution. RGs are hosted by more massive haloes than the C_{M_S} sample, with differences that go from ∼2 dex at z = 1.5 to ∼1.0 dex at z = 3. This is consistent with the results of Mandelbaum et al. (2009), who found that, at fixed stellar mass, radio AGN are found in more massive haloes (1.6×10^{13} M$_\odot$ h^{-1}) than both optical AGNs and the bulk of the galaxy population ($\sim 8 \times 10^{11}$ M$_\odot$ h^{-1}).

The differences between RGs and both control samples are also evident in the $M_{\rm halo} - M_{\rm stellar}$ plane, shown in the second row of Fig. 3. The stellar content of central galaxies increases with halo mass, with a scatter of ∼1.5 dex at fixed halo mass. For the most massive haloes ($M_{\rm halo} \gtrsim 10^{12}$ M$_\odot$ h^{-1}), the relation flattens due to radio-mode AGN feedback. In the range of halo masses in which the RG and C_{M_S} sample overlap, RGs are hosted by galaxies with lower stellar masses than the C_{M_S} galaxies. On the other hand, the C_{M_H} sample matches the median relation of $M_{\rm halo} - M_{\rm stellar}$ for the bulk of the galaxy population (by construction), and RGs display higher stellar masses than those galaxies in the C_{M_H} sample. This implies that RGs have experienced a different mass assembly history

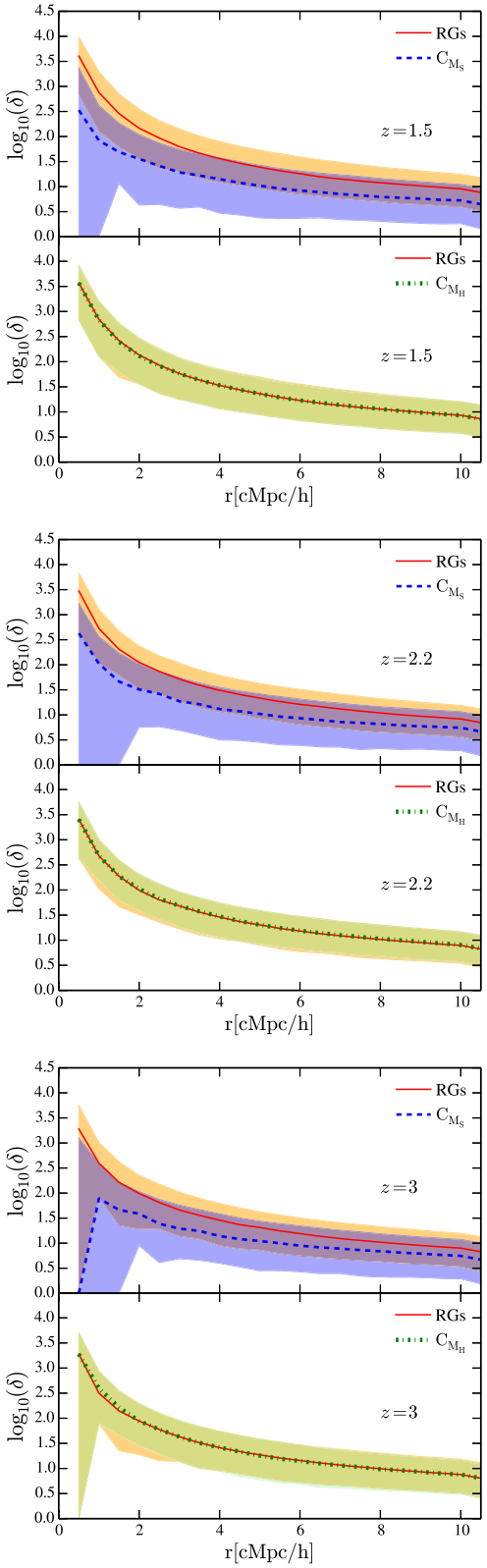

Figure 2. Galaxy overdensities as a function of distance from radio galaxies (red lines) and the galaxies of the C_{M_S} (dashed blue) and C_{M_H} (dotted green) control samples. Results are shown for $z = 1.5$ (top), $z = 2.2$ (middle), and $z = 3$ (bottom panel). The shading represents the values between the 10 and 90 percentiles (orange for the RGs, blue for the C_{M_S} , and green for the C_{M_H}).

compared to typical galaxies with the same host halo mass.[4] This difference seems to smear out towards lower redshifts, especially at the massive end, where the main physical process responsible for star formation quenching is AGN feedback.

In Fig. 3 we also display RGs in terms of their main mode of accretion in to the SMBH. At all redshifts studied, the RG sample is composed of two different populations, the one that experiences *hot-halo* accretion and the one in the *starburst* accretion. In GALFORM, only the *hot-halo* mode of accretion is linked with the AGN feedback phase (see Bower et al. 2006; Lacey et al. 2016). Cold gas accretion in the *starburst* mode occurs after a merger or a disc instability but does not result in the quenching of star formation activity, unlike other semi-analytical models like GAEA (Hirschmann, De Lucia & Fontanot 2016). RGs experiencing hot-halo accretion lie closer to the median relation in the $M_{\rm halo} - M_{\rm stellar}$ plane compared to those experiencing *starburst* accretion. The relative abundance of each mode of accretion varies with redshift. Accretion from the *hot halo* declines towards high redshifts, from ∼50 per cent at $z = 1.5$ to ∼23 per cent at $z = 3.0$. *Hot-halo* accretion dominates at the massive end ($M_{\rm halo} \gtrsim 10^{12.5}$ M$_\odot\, h^{-1}$) of the halo mass function, as it is shown in the first and third row of Fig. 3. Despite that not all the galaxies in the *hot-halo* mode are experiencing AGN feedback, in our redshift range these two conditions are fulfilled by most haloes with masses above $M_{\rm halo} \sim 10^{11.8}$ M$_\odot\, h^{-1}$ (see fig. D1 in Mitchell et al. 2016). Since all our RGs accreting in the *hot-halo* mode have $M_{\rm halo}$ above this threshold regardless of redshift, these are experiencing AGN feedback. The third row of Fig. 3 thus shows that only a fraction of all RGs are indeed experiencing AGN feedback. The remaining RGs are experiencing *starburst*- mode accretion. At low halo masses, the fraction of RGs undergoing *hot-halo* accretion is lower than that from the C_{M_H} sample. At the massive end, *hot-halo* accretion is more common among RGs than in the C_{M_H} sample, since the latter also includes galaxies experiencing no accretion at all.

3.2 Triggering radio galaxies

Although there is not a significant difference in the environment of RGs compared to those from the C_{M_H} sample, RGs are a subsample of galaxies populating massive haloes where powerful radio jet emission has been triggered. By comparing both populations, we explore here the mechanisms that allow powerful radio emission in galaxies.

Fig. 3 shows that an important fraction of the RG sample is triggered by mergers and disc instabilities (starburst mode). This is consistent with the results of Chiaberge et al. (2015), where 92 per cent of their radio-loud objects at $z > 1$ are associated with recent or ongoing merger events. In GALFORM, the starburst mode is activated by mergers and disc instabilities that destroy galaxy discs and are responsible for increasing the bulge mass. Thus, most RGs are bulge-dominated, with a less massive disc component and more massive bulges than the galaxies in the C_{M_H} sample. Furthermore, we find that ∼80 per cent of RGs show ongoing starburst activity

[4]Galaxies selected as RGs have been growing mainly via mergers feeding their black hole in the starburst mode, thus not being affected by AGN feedback processes. At z= 1.5, 2.2, and 3.0 some of them are feeding their black holes during the hot-halo mode, quenching their host galaxy and moving towards a typical $M_{\rm halo} - M_{\rm stellar}$ relation. However, RGs triggered by starburst mode are not following this relation, and are instead consistent with typical star-forming galaxies with $M_{\rm halo} > 10^{12}$ M$_\odot\, h^{-1}$.

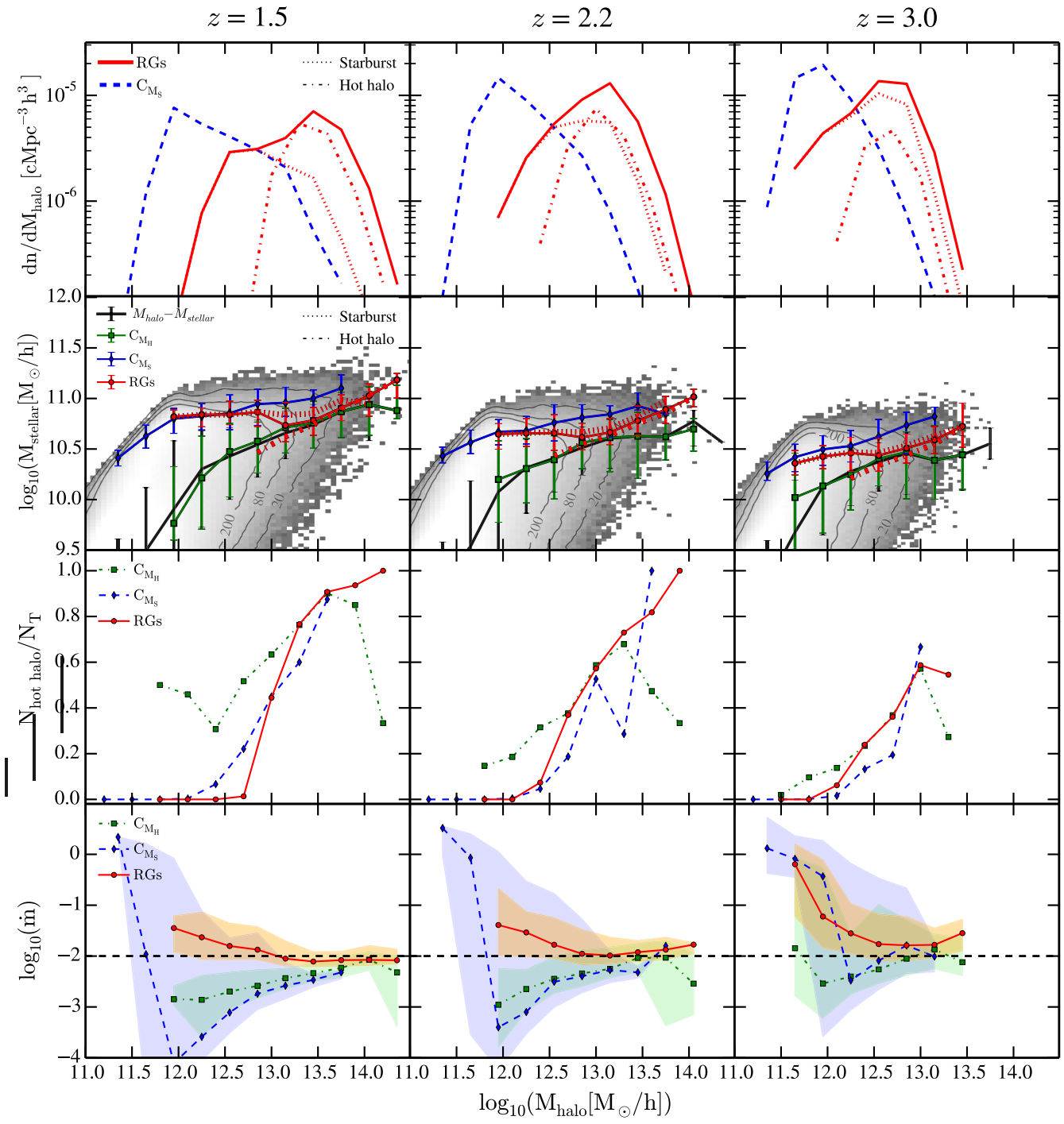

Figure 3. Top row: Halo mass function of RGs (solid red line) and the C_{M_S} galaxies (dashed blue line), at three different redshifts. For the RG host haloes, we show the division between haloes whose BHs are accreting gas from the hot-halo (red dash-dotted line) and starburst mode (red dotted line). Second row: $M_{\rm halo} - M_{\rm stellar}$ relation for central galaxies at $z = 1.5$, 2.2, and 3.0.The black line corresponds to the median stellar mass per halo mass bin for central galaxies. The red curve shows the same for RGs. Blue diamonds and green squares show this for the C_{M_S} and C_{M_H} samples, respectively. The bars represent the 16–84 percentile. The red dotted lines represent the relation for RGs whose BHs are accreting cold gas in the starburst mode while the red dashed-dotted lines the same but for the hot halo regime. The isocontours represent regions of different number of galaxies per $M_{\rm halo} - M_{\rm stellar}$ bin Third row: fraction of galaxies per halo bin that are accreting gas from the hot-halo atmosphere. RGs are shown in red, C_{M_S} in blue, and C_{M_H} in green. Bottom row: The median distribution of specific accretion rates ($\dot{m}$) for RGs (red), C_{M_S} (green), and C_{M_H} (blue) BHs as a function of halo mass. The dashed line represents the critical AGN accretion rate ($\dot{m}_c$) which separates the two accretion regimes in the model: ADAF and TD. The shaded regions represent the 16-84 percentile range.

while only ∼50 per cent of C_{M_H} galaxies are actively star forming at $z = 1.5$, 2.2, and 3.

The specific accretion rate $\dot{m}$ determines the channel of radio power in a galaxy, either via thin disc or ADAF, as discussed in Section 2. The bottom panels of Fig. 3 show the median $\dot{m}$ per bin of halo mass for RGs, C_{M_S}, and C_{M_H}. RGs hosted in the most massive haloes are characterized by the ADAF channel with $\dot{m}$ values distributed around $\dot{m}_c$ (i.e. the maximum radio jet luminosity allowed in the ADAF channel). On the other hand, RGs hosted by less massive haloes, fuelled by starburst accretion, have $\dot{m}$ values that are bigger than $\dot{m}_c$, so their BH accretion is characterized by the TD channel. Regarding the control samples, C_{M_H} is always characterized by an ADAF with lower Eddington rates than RGs. The C_{M_S} median accretion rates are overall associated with the ADAF channel.

In summary, RGs are triggered by both TD and ADAF channels which are fuelled by hot and cold gas from the hot-halo atmosphere and merger/disc instabilities, respectively. The TD channel can trigger a powerful radio-loud jet when the BH in the host RG is very massive ($M_{BH} \gtrsim 10^{8.5}\,M_\odot\,h^{-1}$) and the BH spin is around $a \sim 0.5$. For the ADAF channel, in addition to these constraints, the accretion rate needs to be close to the maximum allowed for an ADAF to occur. Furthermore, RGs triggered by cold gas accretion (*starburst* mode) are more abundant at $z \gtrsim 2.2$ while at lower redshifts, hot gas accretion becomes the main mode of RG triggering.

3.3 The effects of AGN feedback on radio galaxies

As we already discussed, since radio power is linked to AGN activity, it is likely that feedback from accreting black holes is the main physical mechanism responsible for quenching star formation in RGs, thus causing these galaxies to lie in the $M_{halo} - M_{stellar}$ plane closer to the galaxies that have already experienced significant quenching (the massive end). To verify that AGN feedback is responsible for the quenching of the most massive RGs, we run a variant of GALFORM in which AGN feedback is 'switched off', and study the environment of the galaxies that were classified as RGs in the original run. The counterparts of RGs in the new run (hereafter RG^{AGNoff}) are found by matching the position and halo masses of the galaxies in the new run with the ones of RGs in the original run.

We then also generate two new control galaxy samples, matching the stellar masses and the halo masses of the RG^{AGNoff}. We refer to the new control samples as $C_{M_S}^{AGNoff}$ and $C_{M_H}^{AGNoff}$, respectively. We then calculate the overdensities around the three new populations, showing in Fig. 4 the results for $z = 2.2$. In contrast with the results of the original run, now the overdensity profiles around the RG counterparts and the $C_{M_S}^{AGNoff}$ sample (upper panel) are almost identical, indicating that now there are no important differences in the halo masses hosting RG^{AGNoff} and the control sample matched in stellar mass. Consistently, the overdensities around the RG^{AGNoff} sample and the $C_{M_H}^{AGNoff}$ sample (lower panel) are found to be indistinguishable, as in the original model.

This simple test run confirms the idea that the AGN feedback shapes the RG overdensities.

3.4 Comparison with observations

The previous section showed that the environment of radio galaxies can provide information about the effect of AGN feedback on the stellar content of these objects. Here, we compare our model predictions of the overdensities around radio galaxies with recent

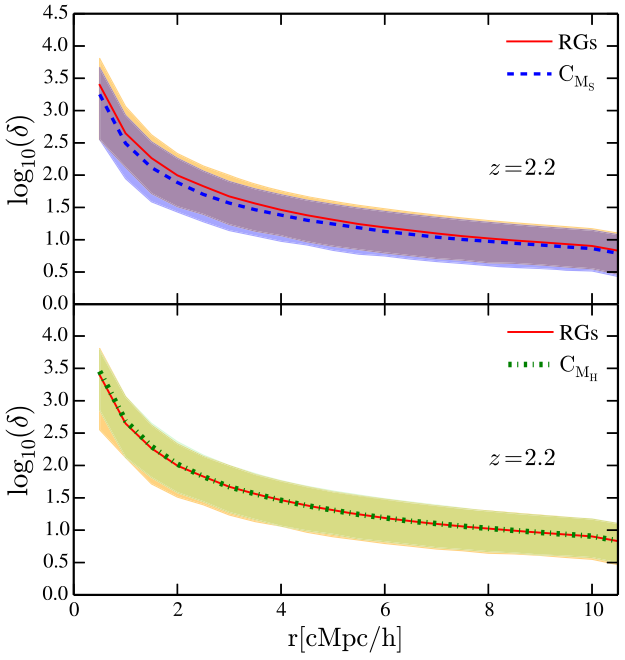

Figure 4. Overdensity around central galaxies when AGN feedback is switched off. The shading represents the values between the 10 and 90 percentiles (orange for RGs, blue for C_{M_S}, and green for C_{M_H}). The two plots show an overdensity comparison around RGs (red), C_{M_S} (dashed blue in top panel), and C_{M_H} (dotted green in the panel below) at $z = 2.2$.

observational results from the CARLA survey (Wylezalek et al. 2013, 2014; Cooke et al. 2015, 2016).

The CARLA survey is a warm *Spitzer* program designed to study the environment of nearly 400 radio-loud sources, of which 187 are radio-loud quasars and 200 are radio galaxies. Targets were selected over the redshift range $1.3 < z < 3.2$. The CARLA AGN sample is composed of powerful RLAGNs whose luminosity at 500 MHz is above $10^{27.5}\,W\,Hz^{-1}$. In order to compare environmental properties, the CARLA team selected a control sample from UKIDSS Ultra Deep Survey (UDS)[5] composed of radio-quiet galaxies[6] with the same stellar mass and redshift distribution. To study the environment of the radio-loud and -quiet sources, they relied on IRAC colour-selected galaxies using IRAC channel 1 (IRAC1) and 2 (IRAC2) with effective wavelengths of 3.55 and 4.49 μm, respectively. Specifically, *Spitzer*-selected sources were define either as sources brighter than the IRAC2 95 per cent completeness limit, above an IRAC1 flux of 2.5μJy (3.5σ detection limit), and with a colour of $[3.6] - [4.5] > -0.1$ or as sources detected above the IRAC2 95 per cent completeness limit, an IRAC1 flux < 2.8μJy, and a colour > −0.1 at the 3.5σ detection limit of the IRAC1 observation (Hatch et al. 2014; Wylezalek et al. 2014). This means that all IRAC-selected sources are 95 per cent complete in the IRAC2 band down to [4.5] = 22.9, but are not necessarily detected in IRAC1. The cuts were performed in order to get a homogeneous sample of field galaxies between $1.3 < z < 3.2$ with a 10–20 per cent contamination level by low-redshift interlopers (Muzzin et al. 2013).

[5]UKIRT Infrared Deep Sky Survey (UKIDSS, Lawrence et al. 2007) Ultra Deep Survey (UDS) is a near-infrared survey covering 0.77 deg^2 in the *J*, *H*, and *K* bands (see Almaini et al. 2017).

[6]Galaxies with radio luminosities at least two orders of magnitude lower than the radio luminosities of CARLA RLAGNs.

Table 1. Number of galaxies in the RG and C_{M_S} samples and the radio luminosity range that RGs display at $\nu = 500$ MHz at $z = 1.5$, $z = 2.2$, and $z = 3$.

z	N_{RG}	$L^{min}_{\nu_{500MHz}}$(W Hz^{-1})	$L^{max}_{\nu_{500MHz}}$ (W Hz^{-1})	$N_{C_{M_S}}$
1.5	1969	9.30×10^{25}	2.45×10^{27}	1969
2.2	2077	8.32×10^{25}	1.57×10^{27}	2077
3	1897	4.95×10^{25}	2.45×10^{27}	1897

To compare with the CARLA results, we selected the 0.1 per cent brightest radio sources at 500 MHz in the GALFORM outputs. We choose this percentage in order to have a large sample of RGs (~ 10 – the CARLA survey) and, at the same time, select only the most powerful radio galaxies in the model. As for the control galaxies, we built a galaxy sample with the same stellar mass distribution as the selected radio galaxies. The number of RGs and galaxies in the control sample at each redshift ($z = 1.5$, 2.2, 3) is presented in Table 1. In order to reproduce the same redshift distribution for the radio sources as the CARLA sample (shown in Hatch et al. 2014), we randomly selected the same number of objects in each redshift bin, using our RGs and control sample at redshift $z = 1.5$ to cover the observed range [1.3–1.8], the $z = 2.2$ sample for the range [1.8–2.5], and the $z = 3$ sample for the range [2.5–3.1].

The sample of field galaxies used to estimate overdensities is selected with the same constraints as are applied in the CARLA survey. To account for the projection effects in observations, we join and stack our three redshift boxes along the z-axis computing the projected overdensities in the same redshift bins analysed by CARLA. In order to remove a large fraction of interlopers, Hatch et al. (2014) excluded sources with [4.5] < 19.1 mag following the results from Wylezalek et al. (2014). To make a fair comparison between our predictions and their observed results, on top of applying the colour selections explained above, we impose this last magnitude cut to select field galaxies.

The large volume of the P-MILLENNIUM simulation allows us to create 33 different mocks that mimic the observational selection of the CARLA survey, which we use to study the impact of cosmic variance. In Fig. 5, we show the ratio of the projected overdensities around radio galaxies and the control sample in the simulation, and compare them with the CARLA survey data. The ratio of projected overdensities measured in the CARLA sample (black dots) is consistent (within the 10–90 percentile range, blue shading in the figure) with our model predictions for $\theta \gtrsim 0.4$ arcmin ($\sim$200 proper kpc at z= 2.2). The slight tension at smaller angular distances can be explained as a result of observational effects like cosmic variance or due to the fact that GALFORM predicts that RGs are hosted by very massive haloes (Fanidakis et al. 2013b; Orsi et al. 2016). However, less massive haloes could fuel powerful radio jets by a variety of mechanisms such as magnetohydrodynamic acceleration near the BH or a transition between ADAF and TD accretion flows (Blandford & Znajek 1977; Wilson & Colbert 1995; Meier 2002; Sikora, Stawarz & Lasota 2007; Beckwith, Hawley & Krolik 2008). Nevertheless, the remarkable agreement shown in Fig. 5 suggests that our physical interpretation of the environments of radio galaxies is a clear signature of the impact of AGN feedback at these high redshifts.

One of the limitations of the CARLA results is the uncertain redshift of the sources used to trace the environments. Ideally, a multi-object spectrograph could be used to systematically identify galaxies at the same redshift as the central object. However, this has only been performed for a small numbers of objects at most (see e.g. Overzier et al. 2001; Venemans et al. 2004; Venemans 2005; Geach et al. 2007; Kuiper et al. 2011). The future survey WEAVE-LOFAR (Smith et al. 2016), which combines radio selection with the new WEAVE spectrograph, will provide a large sample to study the influence of powerful AGNs on their surroundings. Alternatively, narrow-band photometry targeting emission-line objects can detect galaxies in a narrow redshift window that matches the objects of interest. The J-PAS photometric survey (Benitez et al. 2014), for example, is expected to map $\sim$8000 deg^2 of the northern sky with multiple narrow and broad-band filters with a redshift accuracy of $\sigma_z \approx 10^{-3}(1 + z)$.

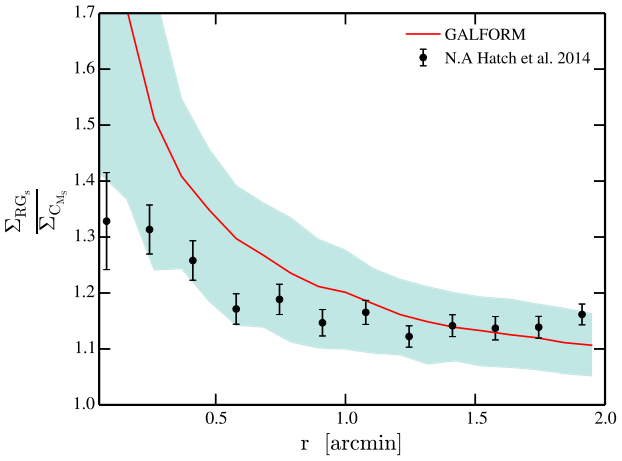

Figure 5. Ratio of the surface density of objects around radio galaxies and around the control sample. The red curve indicates the median of the GALFORM mock predictions, with the 10–90 percentiles shown with the blue area. Black dots: the ratio of radio galaxies and control sample projected overdensity found in Hatch et al. (2014). To guide the reader, for the cosmology assumed in the simulation, 1 arcmin corresponds to $\sim$0.5 proper Mpc at $z = 2.2$ (or 1.63 comoving Mpc).

4 THE QUENCHING OF STAR FORMATION AROUND RADIO GALAXY HALOES

The previous section shows that the properties of RG environments can be explained if these galaxies are hosted by DM haloes about an order of magnitude more massive than their radio-quiet counterparts. In such dense environments, we also expect to find differences in the properties of the galaxies around radio galaxies and the radio-quiet control sample. Environmental mechanisms, such as ram-pressure stripping of gas, have a greater impact in massive haloes (Dressler 1986; Goto et al. 2003; Heinz et al. 2003; Fujita & Goto 2004; Roediger 2009).

In order to explore this further, we look at the fraction f_P of passive galaxies around RGs and in the control samples. We define 'passive' as those galaxies whose sSFR is lower than 10^{-10} yr^{-1}. In Fig. 6, we show f_P computed for both RGs and the control samples as a function of distance r to the central object. The RG and the C_{M_S} and C_{M_H} samples converge to the same f_P at $r < 0.25$ Mpc h^{-1}, meaning that, at these small distances, galaxies are hosted inside the main halo and have therefore undergone the same physical processes. At $z = 3.0$, the median virial radius of RG haloes is 560 kpch^{-1}, at $z = 2.2$ it is 775 kpch^{-1}, and at $z = 1.5$ it is 1000 kpch^{-1} while the median virial radius of the C_{M_S} sample is roughly constant in the three redshift bins with a value of 350 kpc h^{-1}. At $r > 0.25$ Mpc h^{-1}, f_P for the C_{M_S} sample shows a significant

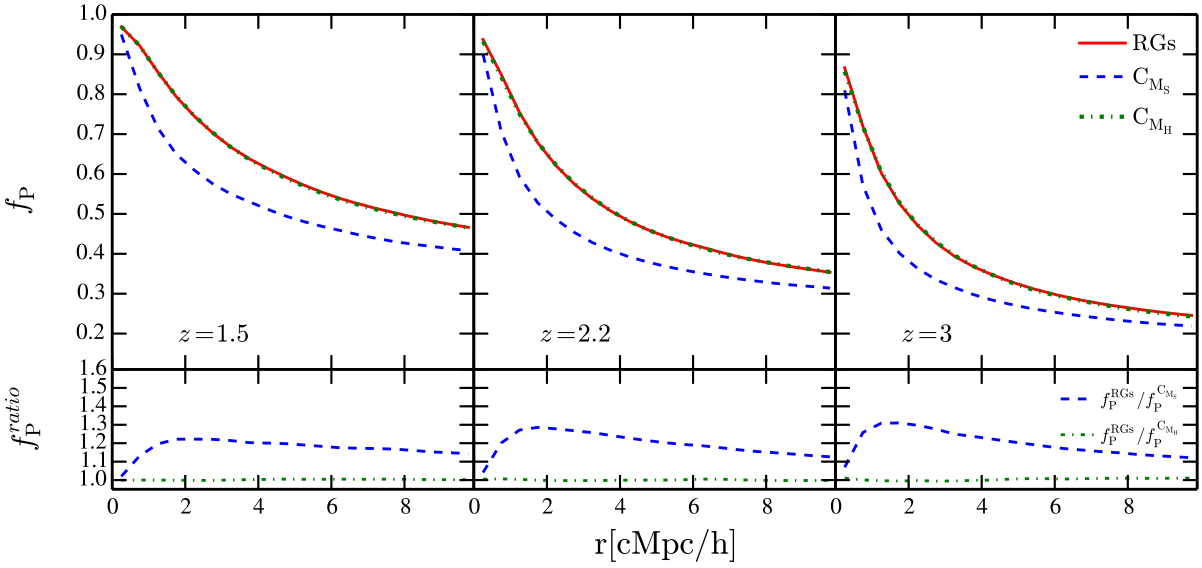

Figure 6. Top panels show the fraction of passive (f_P) galaxies around the RG and control samples (dashed blue line for C_{M_S} and dash dotted green line for C_{M_H}). The left panel is for $z = 1.5$, the middle one is for $z = 2.2$, and the right one is for $z = 3$. The bottom panels show the ratio of fraction of passive galaxies between RGs and the two control samples: C_{M_S} ($f_P^{ratio} = f_P^{RGs} / f_P^{C_{MS}}$) and C_{M_H} ($f_P^{ratio} = f_P^{RGs} / f_P^{C_{M_H}}$).

deviation from the behaviour of the RG and C_{M_H} fractions, which are identical at every redshift. We stress that the quenching around RGs and the C_{M_H} sample is only due to their typical halo mass and not due to the AGN feedback, which only affects the central galaxy.

The bottom panels in Fig. 6 show the radial profiles of the ratio f_P^{ratio} between the values for RGs and C_{M_H} and RGs and C_{M_S} f_P. While the former is flat at any r, the latter increases up to a peak value. At high r, the Δf_P between C_{M_S} and RGs reaches 1, showing that the fraction of passive galaxies in RGs and the C_{M_S} sample converges eventually to the average fraction of passive galaxies in the box. These panels also show that the position of the $f_P^{RGs}/f_P^{C_{M_S}}$ peak depends slightly on redshift. This result is related to the increase of the virial radius of haloes hosting RGs with time.

We further study the properties of the galaxies surrounding RGs by looking at their infrared luminosity function (IRLF), which we can compare with the data from the CARLA survey. Specifically, we compute the total observed IRLF by selecting galaxies inside a radius of 1 arcmin centred on the RGs that meet the selection criteria set out for CARLA objects in Section 3.4. We then measure the IRLF in the three redshift intervals and we compare them with the measurements of Wylezalek et al. (2014). To account for projection effects in the observations, we stack our three redshift boxes spanning $1.5 < z < 3$ along the z-axis. In order to mimic the background subtraction of Wylezalek et al. (2014), we place 500 random and non-overlapping apertures with 1 arcmin of radius onto our projected field to estimate the typical field density of IRAC-selected sources. Then, we compute the average blank field LF and we subtract it from the luminosity function of each RGs. To estimate cosmic variance, we randomly choose 30 RGs from Table1 for each redshift bin to mimic the CARLA sample of RGs.

The results for the predicted IRLF of galaxies around RGs are shown in Fig. 7, together with the measurements from the CARLA survey. The right column corresponds to the luminosity function around RGs and C_{M_S} in the IRAC 1 band with an effective wavelength of 3.55 μm and the left column is the same but in the IRAC 2 band with an effective wavelength of 4.49 μm. Our results are in good agreement with the observations throughout the redshift range $1.5 < z < 3$, except for the brightest bins at the highest z. However, there is a remarkable agreement between the faint end of the observed and predicted LFs suggesting that our predicted RG environments are consistent with the observed ones.

We note that for all redshifts the faint end of the RG LFs is higher than that for C_{M_S}. The fraction of passive galaxies is higher in the RG environments than for C_{M_S} ones. Hence, the *Spitzer* IRLF of objects around the C_{M_S} sample is significantly below the LF of RGs environment, suggesting that the abundance of passive galaxies around these environments is consistent with the observational measurements.

5 SUMMARY AND CONCLUSIONS

Recent observations of radio galaxies have suggested that their environments are denser than those of their radio-quiet counterparts (Hatch et al. 2014). To understand this phenomenon from a theoretical perspective, we use the semi-analytical model of galaxy formation GALFORM (Lacey et al. 2016). This model features a detailed modelling of the co-evolution of galaxies and their central SMBH, including its growth through different accretion channels, spin evolution, and the regulation of star formation through AGN feedback.

We explore the model predictions at redshift 1.5, 2.2, and 3 in which most of the observational work about RG environments has been carried out. In order to analyse the overdensities around radio galaxies, we construct two types of control samples, one with the same stellar mass distribution (C_{M_S}) and the other one with the same halo mass as the RGs (C_{M_H}). Our model predictions are consistent with RGs being in denser environments than galaxies from the C_{M_S} sample, in similar environments to the C_{M_H} sample. The latter suggests that the overdensities around RGs are determined solely by their host halo masses. In fact, RGs are hosted by massive haloes ($10^{11.75} < M_{halo} < 10^{14}$ $M_\odot h^{-1}$) that are on average $\sim$1.5 dex more massive than those from the C_{M_S} sample.

Given that RGs are preferentially hosted by very massive haloes, in which AGN feedback is the most common mechanism to quench

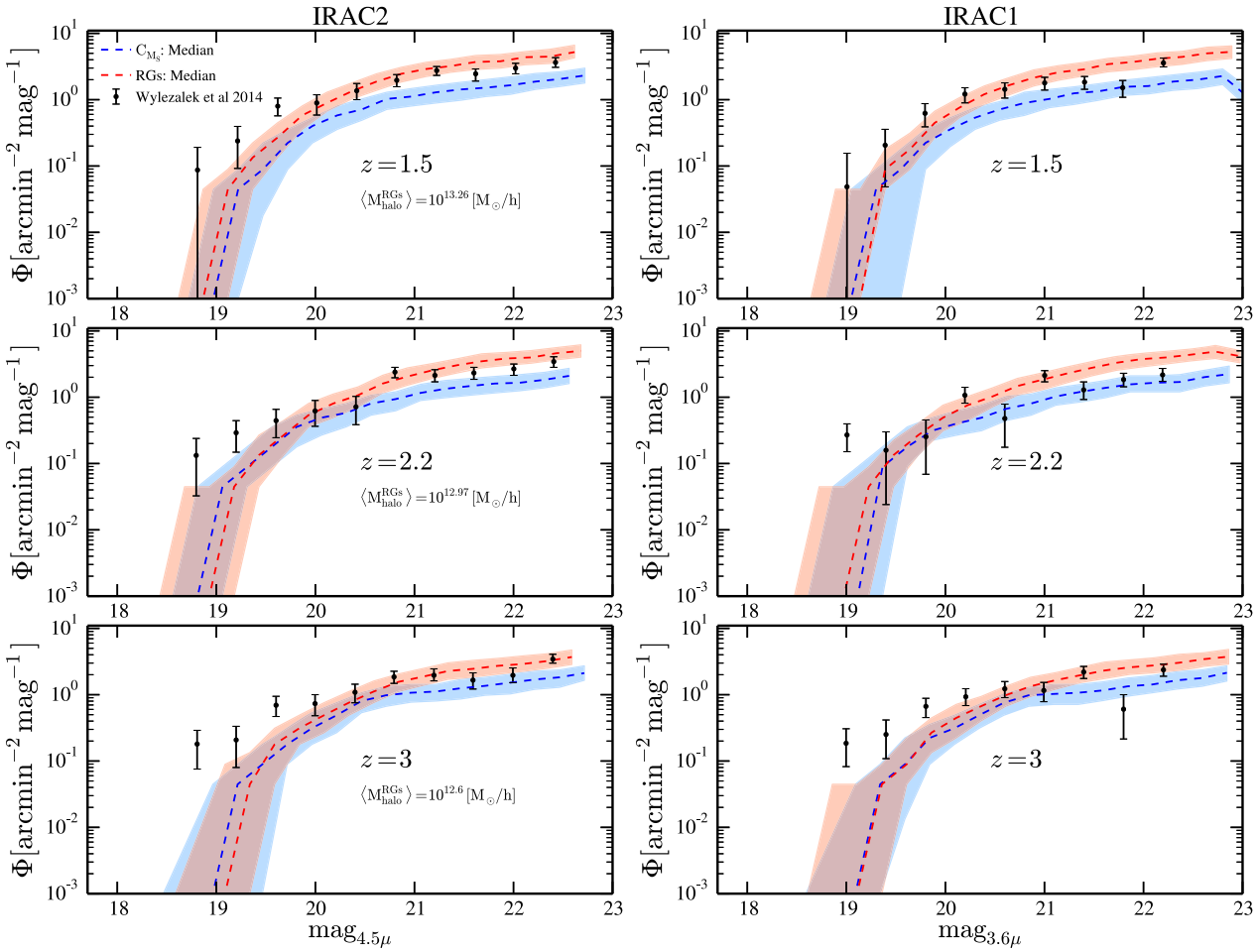

Figure 7. Dashed lines are the LFs in IRAC bands predicted by GALFORM for RG (red) and C_{M_S} (blue) environments, the red and blue shaded regions represent the 10–90 percentiles of the mocks for RGs and C_{M_S} , respectively. The black points show the observational LF of the CARLA sample analysed by Wylezalek et al. (2014). The right column corresponds to the apparent magnitude of sources in the IRAC band 1 with an effective wavelength of 3.55 μm and the left column is the same but in the IRAC band 2 with an effective wavelength of 4.49 μm. The two upper panels show the results in the snapshot redshift $z = 1.5$ and the CARLA sample data in the redshift interval $1.5 < z < 1.9$. The middle panels show are the results in the snapshot redshift $z = 2.2$ and the CARLA sample data in the redshift interval $2.1 < z < 2.3$. And the last bottom panels show the same for the $z = 3$ snapshot and the CARLA sample interval $2.6 < z < 3.1$.

star formation (Bower et al. 2006; Croton et al. 2006), we expect that the RG stellar mass build-up process was slowed down due to the black hole feedback. This would make them be hosted by haloes with less stellar mass with respect to that predicted by the $M_{\rm stellar} - M_{\rm halo}$ relation. In order to test this idea as the main driver of the differences in overdensities around RGs and C_{M_S} , we ran a variant of our model in which AGN feedback is switched off. We find that the halo mass distributions of RGs and the C_{M_S} sample are comparable and they reside in similar environments. These results corroborate the idea that radio galaxies have less stellar mass due to AGN feedback effectively preventing star formation.

Interestingly, we found that while the C_{M_H} sample follows the median relation of $M_{\rm halo} - M_{\rm stellar}$ for the bulk of the galaxy population, RGs lie systematically above this relation, implying that RGs have experienced a different mass assembly history compared to typical galaxies with the same host halo mass. This difference seems to smear out towards lower redshifts, especially at the massive end, where the main physical process responsible for star formation quenching is AGN feedback. To explore the role of this process in shaping the stellar content of radio galaxies, we split them into the ones currently in the *hot-halo* accretion mode and the ones in the *starburst* mode. In the GALFORM model, only the *hot-halo* mode is linked with the AGN feedback (see Lacey et al. 2016). We found that the RG sample is composed of galaxies in these two accretion modes whose relative proportion varies with redshift. Around $\sim$ 23.7 per cent at $z = 3.0$, $\sim$ 43 per cent at $z = 2.2$, and $\sim$ 53.6 per cent at $z = 1.5$ of RG black holes show accretion from the surrounding hot gas atmosphere (i.e, *hot-halo* mode) as the main channel of growth being the principal mode at higher halo masses ($M_{\rm halo} \gtrsim 10^{12}\,{\rm M}_\odot\,h^{-1}$). Only these galaxies, among all RGs, are experiencing feedback from the black hole. On the other hand, the other sample of RG black holes is growing due to cold gas accretion in the *starburst* mode after a merger or a disc instability but is not linked with an AGN feedback phase. Therefore, only a fraction of all RGs are indeed experiencing AGN feedback: At low halo masses, the fraction of RGs experiencing *hot-halo* accretion is low while at the massive end the *hot-halo* accretion is more common among RGs. In addition, the two modes in RGs are preferentially associated with different accretion flow geometries: ADAF is linked to the *hot-halo* mode whereas TD accretion flows are dominant in the *starburst* mode. Both cases, at any redshift, exhibit $\dot{m}$ values close to the critical threshold ∼0.01 in Eddington units.

The versatility of the GALFORM model allows us to compare the predictions against observational measurements of the environments of RGs. We build mock catalogues of the CARLA RG sample (Wylezalek et al. 2013; Hatch et al. 2014). We find remarkable agreement between model predictions and observations when comparing the density of objects around the RGs and the control sample. This supports the physical picture explored here in which the comparison of environments of RGs and their radio-quiet counterparts reveals the effect of AGN feedback at these high redshifts.

Since RGs are hosted by more massive haloes than their radio-quiet counterparts, we expect that the galaxies in their environments experience different transformation mechanisms. This is reflected in the relative fraction of passive galaxies around RGs and around galaxies in the C_{M_S} sample. Galaxies surrounding the C_{M_H} sample have the same fraction of passive as those around RGs. This means that the halo mass distribution is the main property determining the fraction of passive galaxies in the environment of a central object. To validate our model predictions, we compare the observed infrared luminosity function in the *Spitzer* bands (IRAC1 and IRAC2) of RG environments at different redshifts with the observational measurements of the *Spitzer* IRLF in the CARLA survey shown in Wylezalek et al. (2014). The model shows remarkable agreement with the observational data throughout the redshift range $1.5 < z < 3$, except at the brightest bins at the highest redshifts.

Current data samples of environments of high-redshift RGs typically suffer from sample and cosmic variance due to their small size. However, the agreement with our model predictions is encouraging and suggests that future more ambitious observational campaigns could be designed to put constraints on the strength of AGN feedback at high redshifts. For instance, the J-PAS survey is expected to map $\sim$8000 deg^2 of the northern sky with multiple narrow- and broad-band filters with a redshift accuracy of $\sigma_z \approx 10^{-3}(1+z)$ (Benitez et al. 2014). Such a data sample, cross-matched with a high-redshift RG catalogue, would allow us to characterize the environments of these objects with unprecedented accuracy. Likewise, forthcoming multi-object spectroscopic surveys, such as the WEAVE-LOFAR survey (Smith et al. 2016), are expected to increase the number of known RGs at high redshifts and characterize their environments. By comparing the results from these large data samples to galaxy formation model predictions such as the ones presented here, we expect to be able to put tight constraints on the physical mechanisms regulating galaxy formation and evolution at high redshifts.

ACKNOWLEDGEMENTS

We acknowledge encouraging discussions with Dominika Wylezalek that helped in shaping the ideas presented in this paper. We also acknowledge support from project AYA2015-66211-C2-2 of the Spanish Ministerio de Economia, Industria y Competitividad, and also STFC Consolidated Grants ST/L00075X/1 and ST/P000451/1 at Durham University. This work used the DiRAC Data Centric system at Durham University, operated by the Institute for Computational Cosmology on behalf of the STFC DiRAC HPC Facility (www.dirac.ac.uk). This equipment was funded by BIS National E-infrastructure capital grant ST/K00042X/1, STFC capital grants ST/H008519/1 and ST/K00087X/1, STFC DiRAC Operations grant ST/K003267/1 and Durham University. DiRAC is part of the National E-Infrastructure.

REFERENCES

Almaini O. et al., 2017, MNRAS, 472, 1401
Bardeen J. M., Bond J. R., Kaiser N., Szalay A. S., 1986, ApJ, 304, 15
Baugh C. M., Lacey C. G., Frenk C. S., Granato G. L., Silva L., Bressan A., Benson A. J., Cole S., 2005, MNRAS, 356, 1191
Beckwith K., Hawley J. F., Krolik J. H., 2008, ApJ, 678, 1180
Benitez N. et al., 2014, preprint (arXiv:1403.5237)
Benson A. J., Bower R. G., Frenk C. S., Lacey C. G., Baugh C. M., Cole S., 2003, ApJ, 599, 38
Best P. N., 2000, MNRAS, 317, 720
Best P. N., von der Linden A., Kauffmann G., Heckman T. M., Kaiser C. R., 2007, MNRAS, 379, 894
Bîrzan L., Rafferty D. A., McNamara B. R., Wise M. W., Nulsen P. E. J., 2004, ApJ, 607, 800
Bischetti M. et al., 2017, A&A, 598, A122
Blandford R. D., Znajek R. L., 1977, MNRAS, 179, 433
Bonoli S., Mayer L., Kazantzidis S., Madau P., Bellovary J., Governato F., 2016, MNRAS, 459, 2603
Booth C. M., Schaye J., 2009, MNRAS, 398, 53
Bower R. G., Benson A. J., Malbon R., Helly J. C., Frenk C. S., Baugh C. M., Cole S., Lacey C. G., 2006, MNRAS, 370, 645
Campbell D. J. R. et al., 2015, MNRAS, 452, 852
Cattaneo A. et al., 2007, MNRAS, 377, 63
Chamani W., Doerschner S., Schleicher D. R. G., 2017, A&A, 602, A84
Chiaberge M., Gilli R., Lotz J. M., Norman C., 2015, ApJ, 806, 147
Cole S., Lacey C. G., Baugh C. M., Frenk C. S., 2000, MNRAS, 319, 168
Cooke E. A., Hatch N. A., Muldrew S. I., Rigby E. E., Kurk J. D., 2014, MNRAS, 440, 3262
Cooke E. A. et al., 2015, MNRAS, 452, 2318
Cooke E. A. et al., 2016, ApJ, 816, 83
Croton D. J. et al., 2006, MNRAS, 367, 864
Di Matteo T., Springel V., Hernquist L., 2005, Nature, 433, 604
Diamond-Stanic A. M., Rieke G. H., 2012, ApJ, 746, 168
Dressler A., 1986, ApJ, 301, 35
Dubois Y., Peirani S., Pichon C., Devriendt J., Gavazzi R., Welker C., Volonteri M., 2016, MNRAS, 463, 3948
Eisenreich M., Naab T., Choi E., Ostriker J. P., Emsellem E., 2017, MNRAS, 468, 751
Fanidakis N., Baugh C. M., Benson A. J., Bower R. G., Cole S., Done C., Frenk C. S., 2011, MNRAS, 410, 53
Fanidakis N. et al., 2012, MNRAS, 419, 2797
Fanidakis N. et al., 2013a, MNRAS, 435, 679
Fanidakis N., Macciò A. V., Baugh C. M., Lacey C. G., Frenk C. S., 2013b, MNRAS, 436, 315
Fujita Y., Goto T., 2004, PASJ, 56, 621
Gaspari M., Sądowski A., 2017, ApJ, 837, 149
Gaspari M. et al., 2018, ApJ, 854, 167
Geach J. E., Simpson C., Rawlings S., Read A. M., Watson M., 2007, MNRAS, 381, 1369
Georgakakis A. et al., 2011, MNRAS, 418, 2590
Goto T., Yamauchi C., Fujita Y., Okamura S., Sekiguchi M., Smail I., Bernardi M., Gomez P. L., 2003, MNRAS, 346, 601
Granato G. L., Silva L., de Zotti G., Bressan A., Danese L., 2004, in Plionis M., ed., Astrophysics and Space Science Library, Vol. 301, Multiwavelength Cosmology. Kluwer Academic Publishers, Dordrecht, p. 129
Griffin A. J., Lacey C. G., Gonzalez-Perez V., Lagos C. d. P., Baugh C. M., Fanidakis N., 2018, preprint (arXiv:1806.08370)
Guillard P. et al., 2012, ApJ, 747, 95
Hardcastle M. J., Evans D. A., Croston J. H., 2006, MNRAS, 370, 1893
Harrison C. M. et al., 2012, ApJ, 760, L15
Hatch N. A. et al., 2011, MNRAS, 410, 1537
Hatch N. A. et al., 2014, MNRAS, 445, 280
Heinz S., Sunyaev R. A., 2003, MNRAS, 343, L59
Heinz S., Churazov E., Forman W., Jones C., Briel U. G., 2003, MNRAS, 346, 13

Henriques B. M. B., White S. D. M., Thomas P. A., Angulo R., Guo Q., Lemson G., Springel V., Overzier R., 2015, MNRAS, 451, 2663
Hill G. J., Lilly S. J., 1991, ApJ, 367, 1
Hirschmann M., De Lucia G., Fontanot F., 2016, MNRAS, 461, 1760
Holt J., Tadhunter C. N., Morganti R., 2008, MNRAS, 387, 639
Kormendy J., Gebhardt K., 2001, in Wheeler J. C., Martel H., eds, AIP Conf. Proc. Vol. 586, 20th Texas Symposium on Relativistic Astrophysics, Am. Inst. Phys., p. 363
Kormendy J., Richstone D., 1995, ARA&A, 33, 581
Kuiper E. et al., 2011, MNRAS, 415, 2245
Kurk J. D. et al., 2000, A&A, 358, L1
Kurk J., Venemans B., Röttgering H., Miley G., Pentericci L., 2004a, in Plionis M., ed., Astrophysics and Space Science Library, Vol. 301, Multiwavelength Cosmology. Kluwer Academic Publishers, Dordrecht, p. 141
Kurk J. D., Pentericci L., Overzier R. A., Röttgering H. J. A., Miley G. K., 2004b, A&A, 428, 817
Lacey C. G. et al., 2016, MNRAS, 462, 3854
Lagos C. D. P., Cora S. A., Padilla N. D., 2008, MNRAS, 388, 587
Lanzuisi G. et al., 2017, A&A, 602, A123
Lawrence A. et al., 2007, MNRAS, 379, 1599
Malbon R. K., Baugh C. M., Frenk C. S., Lacey C. G., 2007, MNRAS, 382, 1394
Mandelbaum R., Li C., Kauffmann G., White S. D. M., 2009, MNRAS, 393, 377
Meier D. L., 2002, New Astron. Rev., 46, 247
Mitchell P. D., Lacey C. G., Baugh C. M., Cole S., 2016, MNRAS, 456, 1459
Morganti R., Fogasy J., Paragi Z., Oosterloo T., Orienti M., 2013, Science, 341, 1082
Mullaney J. R. et al., 2012a, MNRAS, 419, 95
Mullaney J. R. et al., 2012b, MNRAS, 419, 95
Mullaney J. R. et al., 2012c, ApJ, 753, L30
Muzzin A., Wilson G., Demarco R., Lidman C., Nantais J., Hoekstra H., Yee H. K. C., Rettura A., 2013, ApJ, 767, 39
Narayan R., Yi I., 1994, ApJ, 428, L13
Nesvadba N. P. H., Lehnert M. D., De Breuck C., Gilbert A. M., van Breugel W., 2008, A&A, 491, 407
Nesvadba N. P. H., De Breuck C., Lehnert M. D., Best P. N., Collet C., 2017, A&A, 599, A123
Orsi Á. A., Fanidakis N., Lacey C. G., Baugh C. M., 2016, MNRAS, 456, 3827
Overzier R. A., Röttgering H. J. A., Kurk J. D., De Breuck C., 2001, A&A, 367, L5
Pascarelle S. M., Windhorst R. A., Driver S. P., Ostrander E. J., Keel W. C., 1996, ApJ, 456, L21
Perucho M., Quilis V., Martí J.-M., 2011, ApJ, 743, 42
Perucho M., Martí J.-M., Quilis V., Ricciardelli E., 2014, MNRAS, 445, 1462
Planck Collaboration XIII, 2016, A&A, 594, A13
Richstone D. et al., 1998, Nature, 395, A14
Rodighiero G. et al., 2015, ApJ, 800, L10
Roediger E., 2009, Astron. Nachr., 330, 888
Seymour N. et al., 2007, ApJS, 171, 353
Shabala S. S., Deller A., Kaviraj S., Middelberg E., Turner R. J., Ting Y. S., Allison J. R., Davis T. A., 2017, MNRAS, 464, 4706
Shakura N. I., Sunyaev R. A., 1973, A&A, 24, 337
Shao L. et al., 2010, A&A, 518, L26
Sikora M., Stawarz Ł., Lasota J.-P., 2007, ApJ, 658, 815
Silk J., Rees M. J., 1998, A&A, 331, L1
Simha V., Cole S., 2017, MNRAS, 472, 1392
Smith D. J. B. et al., 2016, in Reylé C., Richard J., Cambrésy L., Deleuil M., Pécontal E., Tresse L., Vauglin I., eds, SF2A-2016: Proceedings of the Annual Meeting of the French Society of Astronomy and Astrophysics, held in Centre de Recherche Astrophysique de Lyon, 2016 June 14–17, p. 271
Soergel B., Giannantonio T., Efstathiou G., Puchwein E., Sijacki D., 2017, MNRAS, 468, 577
Soltan A., 1982, MNRAS, 200, 115
Somerville R. S., Hopkins P. F., Cox T. J., Robertson B. E., Hernquist L., 2008, MNRAS, 391, 481
Spinoso D., Bonoli S., Dotti M., Mayer L., Madau P., Bellovary J., 2017, MNRAS, 465, 3729
Springel V., 2005, MNRAS, 364, 1105
Stanley F., Harrison C. M., Alexander D. M., Swinbank A. M., Aird J. A., Del Moro A., Hickox R. C., Mullaney J. R., 2015, MNRAS, 453, 591
Tchekhovskoy A., 2015, in Contopoulos I., Gabuzda D., Kylafis N., eds, Astrophysics and Space Science Library Vol. 414, The Formation and Disruption of Black Hole Jets. Springer International Publishing, Switzerland, p. 45
Venemans B. P., 2005, PhD thesis, Leiden Observatory, Leiden University, the Netherlands
Venemans B. P. et al., 2004, A&A, 424, L17
Wagner A. Y., Bicknell G. V., 2011, ApJ, 728, 29
Wagner A. Y., Bicknell G. V., Umemura M., 2012, ApJ, 757, 136
Wagner A. Y., Umemura M., Bicknell G. V., 2013, ApJ, 763, L18
Weinberger R. et al., 2017, MNRAS, 465, 3291
Wilson A. S., Colbert E. J. M., 1995, ApJ, 438, 62
Wylezalek D. et al., 2013, ApJ, 769, 79
Wylezalek D. et al., 2014, ApJ, 786, 17
Zamaninasab M., Clausen-Brown E., Savolainen T., Tchekhovskoy A., 2014, Nature, 510, 126

APPENDIX A:

Here we explore the effect of galaxy selection around RGs, C_{M_S}, and C_{M_H} on their respective overdensities. We select field galaxies under a different stellar mass cut ($M_{\rm stellar} > 10^{10}\,{\rm M}_{\odot}\,h^{-1}$) with respect to the one used in the main analysis (see Section 3.1). The results presented in Fig. A1 are computed with the method explained in Section 3.1. As we can see, the overdensities are indistinguishable from those presented in Fig. 2. This means that the mass cut used to define field galaxies is not contributing to the overdensities measured around RGs.

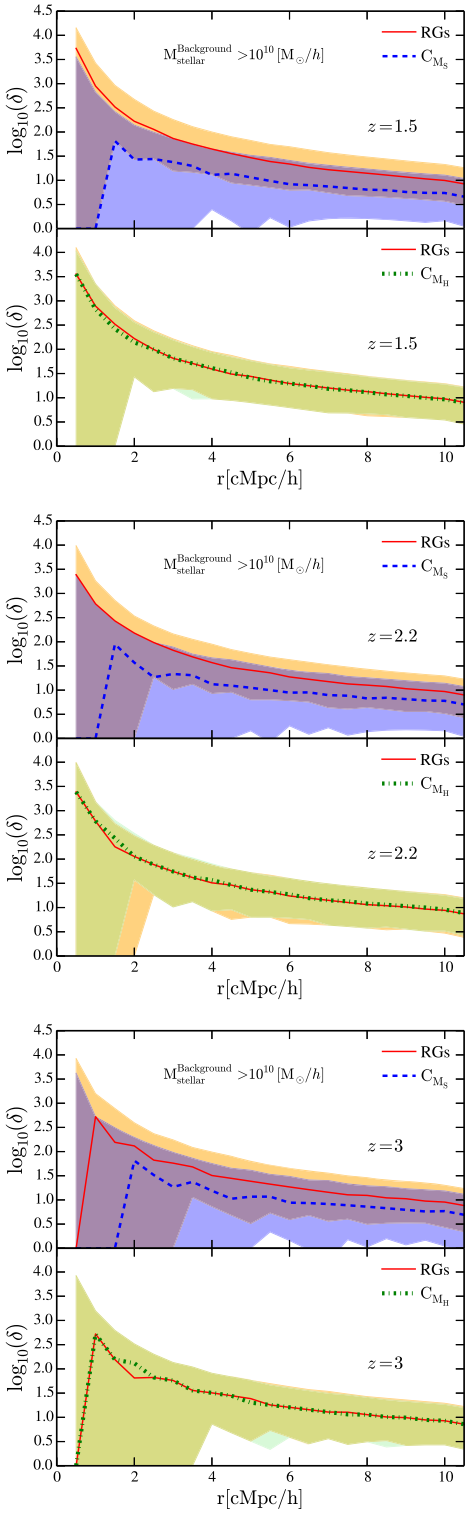

Figure A1. Galaxy overdensities as a function of distance from radio galaxies (red lines) and the galaxies of the C_{M_S} (dashed blue) and C_{M_H} (dotted green) control samples. The galaxies used to compute the average number density of galaxies across the simulation box have $M_{stellar} > 10^{10}\,M_\odot\,h^{-1}$. Results are shown for $z = 1.5$ (top), $z = 2.2$ (middle), and $z = 3$ (bottom panel). The shading represents the values between the 10 and 90 percentiles (orange for the RGs, blue for the C_{M_S} , and green for the C_{M_H}).

This paper has been typeset from a TEX/LATEX file prepared by the author.